

Strong $3p$ - T_{1u} hybridization in $\text{Ar}@C_{60}$ M. Morscher,¹ A. P. Seitsonen,² S. Ito,³ H. Takagi,³ N. Dragoe,⁴ and T. Greber^{1,*}¹*Physik-Institut, Universität Zürich, Winterthurerstrasse 190, CH-8057 Zürich, Switzerland*²*Physikalisch-Chemisches Institut, Universität Zürich, Winterthurerstrasse 190, CH-8057 Zürich, Switzerland, and IMPMC, CNRS and Université Pierre et Marie Curie, 4 place Jussieu, case 115, F-75015 Paris Cedex 05, France*³*Department of Advanced Materials, University of Tokyo, Kashiwa-no-ha 5-1-5, Kashiwa 277-8561, Japan*⁴*Laboratoire d'Étude des Matériaux Hors Équilibre (LEMHE-ICMMO), UMR 8182-CNRS, Université Paris Sud, F-91405 Orsay, France*

(Received 1 July 2010; published 29 November 2010)

Multilayers of fullerenes with and without endohedral Ar units, $\text{Ar}@C_{60}$ and C_{60} , were investigated by photoemission and density-functional theory. The stoichiometry and the endohedral nature of Ar were checked by x-ray photoelectron spectroscopy and x-ray photoelectron diffraction. Valence-band ultraviolet photoemission spectra showed a strong hybridization of the Ar $3p$ valence shell with the $6T_{1u}$ molecular orbital of C_{60} . A hybridization gap of 1.6 ± 0.2 eV was found. This is in agreement with density-functional theory, which predicts 1.47 eV and indicates that $\text{Ar}@C_{60}$ is a noble gas compound with a strong coupling between Ar and the C_{60} cage. No giant Ar photoemission cross section as previously predicted for the gas phase in Phys. Rev. Lett. **99** 243003 (2007) was found.

DOI: [10.1103/PhysRevA.82.051201](https://doi.org/10.1103/PhysRevA.82.051201)

PACS number(s): 61.48.-c, 71.20.Tx, 33.60.+q, 61.05.js

Shortly after the discovery of C_{60} [1], it was proposed that fullerene carbon cages could be filled with other atoms or molecules [2]. The realization of such molecules, called endofullerenes or incar-fullerenes, was expected to lead to new functionalities, where the endohedral units are isolated by the carbon cage from the surroundings. Single nitrogen atoms in C_{60} are a prominent example [3], where the paramagnetic nature of atomic nitrogen even led to the idea of using $\text{N}@C_{60}$ as a qubit [4].

Nuclear magnetic resonance [5] and electron-spin resonance [3] were the first probes of the interior of fullerenes, and photoemission allowed the determination of the valency of endohedral units [6]. The first view inside endofullerenes came from spectacular transmission electron microscopy experiments on so-called peapods, where single Gd atoms that were seen inside C_{82} were lined up in a single-wall nanotube [7]. Only recently, x-ray photoelectron diffraction allowed a direct look at the arrangement of Dy_3N inside C_{80} [8].

Fullerenes containing noble gases were particularly useful for studies on the influence of the endohedral unit on the molecular properties [5,9] and vice versa. There are extended x-ray-absorption fine-structure [10] and x-ray-diffraction experiments [11] on $\text{Kr}@C_{60}$. For $\text{Ar}@C_{60}$, it was shown, for example, that in $\text{K}_3\text{Ar}@C_{60}$ samples the superconducting transition temperature decreased compared to K_3C_{60} [12]. It was also predicted that the dynamic coupling between Ar and the C_{60} cage would lead, near the C_{60} plasmon frequency, to a giant photoemission cross-section enhancement [13].

All these phenomena call for a better understanding of the coupling between the endohedral unit and the fullerene cage. In this Rapid Communication, we explore $\text{Ar}@C_{60}$ layers by means of photoemission, where a comparison with C_{60} allows the quantitative determination of the hybridization between

Ar and C_{60} . The hybridization turns out to be larger than the Ar valence-band width in condensed Ar, which establishes $\text{Ar}@C_{60}$ as a noble gas compound.

Photoemission experiments rely on highly purified samples. For endohedral fullerenes, the synthesis is difficult due to the low production yield and the many purification cycles using high-pressure liquid chromatography. Several milligrams of $\text{Ar}@C_{60}$ have been produced with a purity $>95\%$ [12]. To efficiently deposit the molecules on a substrate, we employed a custom-made evaporator with mini Knudsen cells that can be closely approached to the sample (~ 2 – 3 cm). This allows the preparation of layers from small amounts of material. We used about $10 \mu\text{g}$ of $\text{Ar}@C_{60}$. The experiments were performed in a modified VG ESCALAB 220 photoemission spectrometer with a base pressure of $< 5 \times 10^{-10}$ mbar [14]. All data were measured at room temperature. As a substrate, we used an Al(111) single crystal that was cleaned by repeated cycles of neon ion sputtering (15 min, 1 keV, $\sim 1.5 \mu\text{A}/\text{cm}^2$) and annealing to ~ 700 K. The coverages and the cleanliness of the samples were examined with x-ray photoelectron spectroscopy (XPS). The molecular ordering and the endohedral position of argon were evidenced by x-ray photoelectron diffraction (XPD) [15]. Valence-band photoemission spectra were recorded with monochromatized He $I\alpha$ radiation ($\hbar\omega = 21.2$ eV). Experiments with layers between 3 and 7 monolayers of C_{60} or $\text{Ar}@C_{60}$ have been performed.

The gas-phase geometric and electronic structure of $\text{Ar}@C_{60}$ and C_{60} was determined using density-functional theory (DFT) and the wave-function-based Moller-Plesset method (MP2) with the computer code TURBOMOLE [16]. The Gaussian basis set triple-zeta valence double polarization [17] was used in both calculations, and the exchange-correlation functionals employed in the DFT calculations were the local-density approximation (LDA) and PBE0 [18]. We obtain Ar $3p$ C_{60} T_{1u} hybridization gaps of 1.46, 1.69, and 1.45 eV for PBE0, MP2, and LDA, respectively. In contrast to the calculations in

*greber@physik.uzh.ch

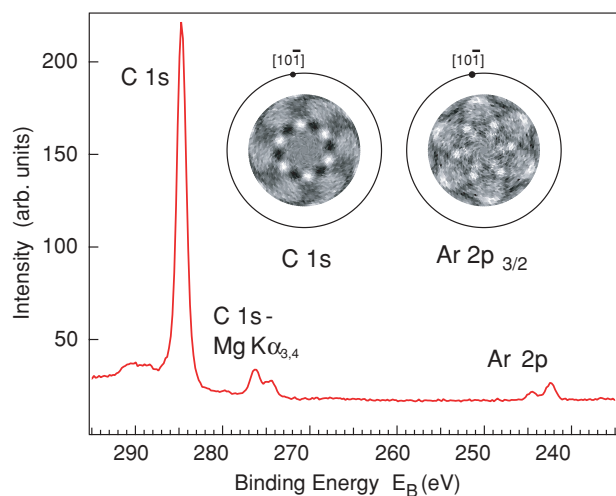


FIG. 1. (Color online) Mg $K\alpha$ XPS and corresponding angle-scanned XPD pattern of $\text{Ar}@C_{60}$. XPS indicates a film thickness of seven monolayers and a C:Ar stoichiometry of $(63 \pm 2) : 1$. The C $1s$ ($E_B = 284.7$ eV) and Ar $2p_{3/2}$ ($E_B = 242.4$ eV) XPD patterns show azimuthal ordering of the molecules, where the high anisotropy ratio between Ar $2p$ and C $1s$ indicates that Ar sits inside the carbon cages.

Ref. [13] where the 240 carbon valence electrons are treated as jellium in a spherical shell, here the full atomic structure is taken into account.

Figure 1 shows the characterization of an $\text{Ar}@C_{60}$ layer on Al(111). The x-ray photoelectron spectrum consists of a dominant C $1s$ and a weak Ar $2p$ peak. From the intensity ratio and the atomic cross sections, a C:Ar atomic ratio of $(56 \pm 7) : 1$ is inferred from two different preparations. This is consistent with the nominal stoichiometry of $\text{Ar}@C_{60}$ and indicates no significant contribution of contaminations containing carbon, such as, for example, C_{60} molecules from an incomplete purification process. In contrast to early reports [19], no evidence for depletion of argon was found under Mg $K\alpha$ and He $I\alpha$ radiation. As for $\text{Dy}_3\text{N}@C_{80}$ on Cu(111) [8],

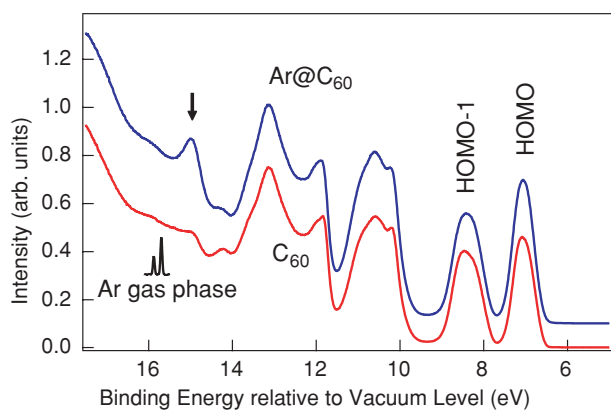


FIG. 2. (Color online) He $I\alpha$ excited normal emission spectra of $\text{Ar}@C_{60}$ (blue upper curve), C_{60} (red lower curve), and gas phase Ar (black inset). The energies refer to the vacuum level. The arrow at 15 eV indicates the Ar peak in the $\text{Ar}@C_{60}$ spectrum, which lies, due to better screening of the photoemission final state, above the Ar $3p$ gas-phase lines.

the XPD patterns in Fig. 1 have sixfold rotational symmetry for the carbon cage as well as for the endohedral unit. The anisotropy of the Ar signal is 6.8 times larger than that of the carbon pattern. As for nitrogen in $\text{Dy}_3\text{N}@C_{80}$ [8], this indicates Ar in the center of C_{60} , which was confirmed by scattering simulations of 60 carbon emitters compared with the pattern of a single emitter in the center of C_{60} .

Figure 2 shows the valence-band photoemission spectra of multilayers of C_{60} and $\text{Ar}@C_{60}$. The two spectra look similar and are dominated by the molecular orbitals of the C_{60} cages. The energies are referenced with respect to the vacuum level, and no significant energy shift between the highest occupied molecular orbital (HOMO) of C_{60} and $\text{Ar}@C_{60}$ is observed. However, at about 15 eV, $\text{Ar}@C_{60}$ has a clear additional feature. As the inset shows, the energy is close to the Ar $3p$ levels in the gas phase, with an ionization potential of 15.76 eV. Endohedral Ar has a lower $3p$ binding energy and a larger peak width (0.53 eV) than in the gas phase where the spin-orbit splitting of 177 meV [20] is resolved. In line with photoemission from condensed Ar [20,21], this indicates a better screening and a significant coupling of the photoemission final state to the many degrees of freedom in the molecule. There is also an indirect indication on the endohedral species: The partial cross-section ratio between the two molecular orbitals HOMO and HOMO-1 is 0.96 ± 0.02 and 0.84 ± 0.01 for $\text{Ar}@C_{60}$ and C_{60} , respectively. In view of the known oscillations of the partial photoemission cross sections [22,23] and its understanding [24], this is an indication that the potential of the endohedral unit influences the phase of photoelectrons from different molecular orbitals differently. The intensity of the Ar-induced feature, however, does not confirm a giant photoemission cross section as predicted by theory, where it was argued that the coupling of the photon to the C_{60} and the Ar cage could enhance the cross section due to resonant interchannel coupling between the Ar $3p$ and the C_{60} photoemission channels [13].

In order to better understand the coupling between the endohedral unit and the C_{60} cage, we performed DFT calculations that yield the eigenvalues and symmetries of the C_{60} and $\text{Ar}@C_{60}$ molecular orbitals. The expectation that the Ar $3p$ level only interacts with molecular orbitals with the corresponding symmetry (T_{1u}) with similar energy and overlap is confirmed nicely. Figure 3 shows calculated PBE0 eigenvalues of C_{60} and $\text{Ar}@C_{60}$. Up to $6T_{1u}$ with the same symmetry as the Ar $3p$ level, the C_{60} orbitals are unaffected by Ar; that is, they have energy differences for C_{60} and $\text{Ar}@C_{60}$ below 25 meV. In C_{60} , $5T_{1u}$ is an orbital with σ bond character and shows no hybridization (less than 1 meV) due to the lack of overlap. The $6T_{1u}$ orbital with π character and the nearby Ar $3p$ orbital hybridize in $\text{Ar}@C_{60}$ into a bonding orbital (B) and an antibonding orbital (AB), split by 1.47 eV. This indicates a strong hybridization between the endohedral Ar unit and the C_{60} cage. The $2A_g$ orbital of C_{60} at an energy of 27.62 eV is not shown in Fig. 3. Theory predicts a 455-meV $3s-2A_g$ hybridization, though these energy levels are experimentally not accessible with He $I\alpha$ radiation.

If we want to compare the theoretical prediction with the experiment, we first have to assign the Ar peak (see Fig. 2) to the B or the AB orbital. For this purpose, the theoretical molecular orbital eigenvalues are correlated with

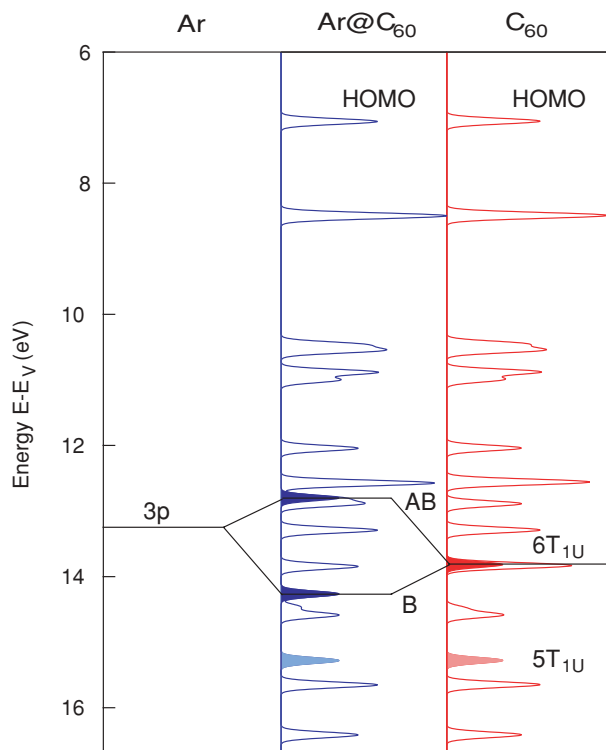


FIG. 3. (Color online) Energy eigenvalues (PBE0) of molecular orbitals of C_{60} and $\text{Ar}@C_{60}$ as calculated with DFT. The orbital energies refer to the vacuum level E_V and are broadened by a Gaussian with 100-meV full width at half maximum. The orbitals with T_{1u} symmetry are solid. In C_{60} , $5T_{1u}$ is a σ orbital and $6T_{1u}$ a π orbital. $6T_{1u}$ hybridizes with the Ar $3p$ shell into a B and an AB orbital with a theoretical splitting of 1.47 eV.

the experimentally observed molecular orbital peaks [25]. If we assume the deviation between theory and experiment to be proportional to the energy [25], the PBE0 results suggest that the experimental Ar peak is 0.64 eV more strongly bound than the calculated B orbital. This difference between experiment and theory is 2.16 eV when we assign the AB orbital to the Ar peak at 14.95 eV. For MP2 calculations, B also fits with a corresponding difference of -0.57 eV better in the experiment than AB, where the difference is 1.25 eV. We therefore assign the experimentally distinct Ar peak to the Ar $3p$ - C_{60} $6T_{1u}$ bonding hybrid B. For the experiment, this means that the antibonding $3p$ - $6T_{1u}$ hybrid orbital must have a lower binding energy than the Ar peak and that the $6T_{1u}$ orbital of C_{60} must lie in between them. A closer inspection of the spectra in Fig. 2 shows that this is the case. The corresponding region of interest is shown in Fig. 4(a). In order to quantify the difference between the two spectra, we show the asymmetry $A = [I(\text{Ar}@C_{60}) - I(C_{60})]/[I(\text{Ar}@C_{60}) + I(C_{60})]$ between the $\text{Ar}@C_{60}$ and the C_{60} spectrum in Fig. 4(b). Clearly, the Ar peak (B) has the largest asymmetry, and at 1.6 eV above this line a new peak shows up. Between the two $\text{Ar}@C_{60}$ peaks, a C_{60} peak (with a local asymmetry minimum) is seen. With this we can identify the $3p$ - $6T_{1u}$ AB hybrid and the $6T_{1u}$ C_{60} molecular orbital. The asymmetry curve in Fig. 4(b) is not flat below B and above AB. This is likely related to the fact that the photoemission cross sections of all other molecular

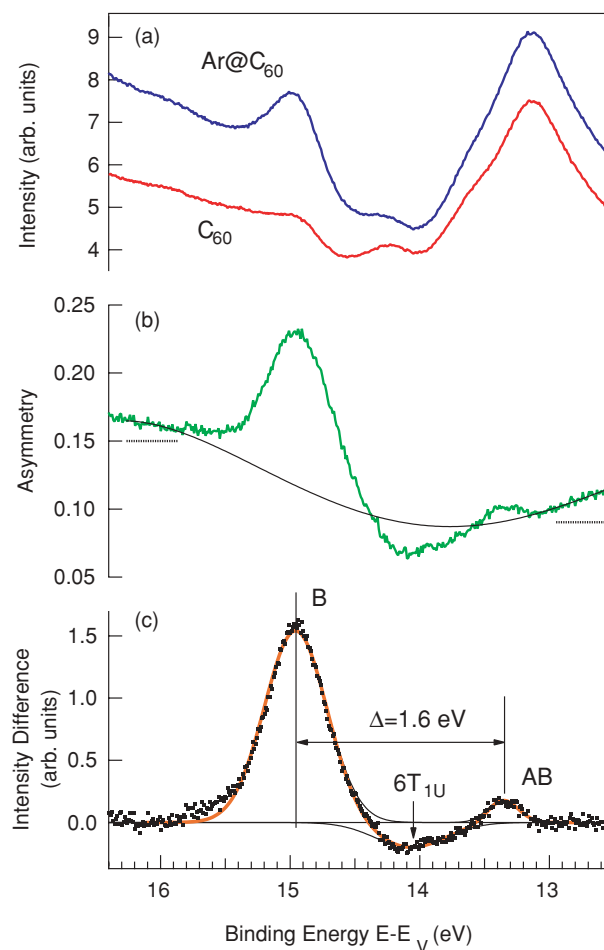


FIG. 4. (Color online) Experimental evidence for the $3p$ - T_{1u} hybridization in $\text{Ar}@C_{60}$ (blue) by comparison with C_{60} (red). (a) Raw data as extracted from the spectra in Fig. 2. (b) Asymmetry between $\text{Ar}@C_{60}$ and C_{60} (green) and the background that has been subtracted for quantification. The dashed horizontal lines are the supporting points of the background polynomial. (c) Difference between $\text{Ar}@C_{60}$ and C_{60} from (a) and the asymmetry in (b) without background. The splitting Δ between the bonding and the antibonding hybrid is 1.6 ± 0.2 eV. The negative part of the difference indicates the $6T_{1u}$ orbital of empty C_{60} .

orbitals are affected by the endohedral unit, as seen in the different HOMO:(HOMO-1) intensity ratios.

In order to quantify the difference between $\text{Ar}@C_{60}$ and C_{60} , we subtract a fourth-order polynomial background from the asymmetry curve in Fig. 4(b) and reconstruct the difference between the $\text{Ar}@C_{60}$ and C_{60} spectrum. In Fig. 4(c), this difference shows a splitting Δ between B and AB of 1.6 ± 0.2 eV, which is close to the calculated value of 1.47 eV. As expected, the hybridizing $6T_{1u}$ molecular orbital of C_{60} shows up with negative values in the intensity difference between $\text{Ar}@C_{60}$ and C_{60} . It lies 0.7 eV below AB, or 0.9 eV above B. This suggests that AB has more $6T_{1u}$ character and correspondingly B more Ar $3p$ character. If $6T_{1u}$ would lie in the middle between B and AB, no big difference between the intensity of B and AB would be expected. The ratio between the B and AB intensity depends on the position in the hybridization gap. Together with the fact that the He $I\alpha$ photoemission cross

section is larger for an Ar $3p$ electron than for a C $2p$ electron, this is consistent with the observation that B has a stronger cross section than AB.

Finally, we would like to discuss the absolute photoemission cross sections of the different molecular orbitals. For the ten HOMO electrons of C_{60} , the experimental photoemission cross section at 21-eV photon energy is 100 and 50 Mb for the gas phase [26] and condensed C_{60} [27], respectively. Comparison of these cross sections with that of atomic C $2p$ ($1.5 \text{ Mb}/e^-$) [28] suggests for the molecule a C $2p$ cross-section enhancement of a factor 7 to 3. The data shown in Fig. 4 allow a comparison of the $Ar@C_{60}$ hybrid orbital cross section, which turns out to be 0.44 ± 0.05 times that of the HOMO and is close to the value of 38 Mb for the Ar $3p$ level [28]. This corresponds to the values as expected from the semiclassical result, and thus we have no indication of a giant cross-section enhancement in low-energy photoemission

of Ar in solid $Ar@C_{60}$, as was proposed for the gas phase [13]. A possible source for the discrepancy might be the energy of the plasmon excitation. In Ref. [13], the giant enhancement is assigned to a redistribution of oscillator strength between a plasmon of C_{60} at 16.5 eV and the close-lying Ar $3p$ level at 15.76 eV. However, the experimental plasmon excitation for C_{60} is about 20 eV in the gas phase, while it shifts to 28 eV in the bulk [29], and a possible resonance between Ar and the C_{60} cage is likely detuned.

In conclusion, it is shown that in $Ar@C_{60}$, the Ar $3p$ and the $C_{60} 6T_{1u}$ orbital strongly hybridize. This coupling between the endohedral unit and the carbon cage establishes $Ar@C_{60}$ as a noble gas compound.

Technical support by Martin Klöckner is gratefully acknowledged. The project was financially supported by the Swiss National Science Foundation.

-
- [1] H. W. Kroto, J. R. Heath, S. C. O'Brien, R. F. Curl, and R. E. Smalley, *Nature (London)* **318**, 162 (1985).
- [2] J. R. Heath, S. C. O'Brien, Q. Zhang, Y. Liu, R. F. Curl, H. W. Kroto, F. K. Tittel, and R. E. Smalley, *J. Am. Chem. Soc.* **107**, 7779 (1985).
- [3] T. Almeida Murphy, T. Pawlik, A. Weidinger, M. Höhne, R. Alcalá, and J. M. Spaeth, *Phys. Rev. Lett.* **77**, 1075 (1996).
- [4] W. Harneit, *Phys. Rev. A* **65**, 032322 (2002).
- [5] M. Saunders, H. A. Jiménez-Vázquez, R. J. Cross, S. Mroczkowski, M. L. Gross, D. E. Giblin, and R. J. Poreda, *J. Am. Chem. Soc.* **116**, 2193 (1994).
- [6] T. Pichler, M. S. Golden, M. Knupfer, J. Fink, U. Kirbach, P. Kuran, and L. Dunsch, *Phys. Rev. Lett.* **79**, 3026 (1997).
- [7] K. Suenaga, T. Tence, C. Mory, C. Colliex, H. Kato, T. Okazaki, H. Shinohara, K. Hirahara, S. Bandow, and S. Iijima, *Science* **290**, 2280 (2000).
- [8] M. Treier, P. Ruffieux, R. Fasel, F. Nolting, S. F. Yang, L. Dunsch, and T. Greber, *Phys. Rev. B* **80**, 081403 (2009).
- [9] M. Saunders, R. J. Cross, H. A. Jiménez-Vázquez, R. Shimshi, and A. Khong, *Science* **271**, 1693 (1996).
- [10] S. Ito, A. Takeda, T. Miyazaki, Y. Yokoyama, M. Saunders, R. J. Cross, H. Takagi, P. Berthet, and N. Dragoe, *J. Phys. Chem. B* **108**, 3191 (2004).
- [11] H. M. Lee, M. M. Olmstead, T. Suetsuna, H. Shimotani, N. Dragoe, R. J. Cross, K. Kitazawa, and A. L. Balch, *Chem. Commun.* 1352 (2002).
- [12] A. Takeda *et al.*, *Chem. Commun.* 912 (2006).
- [13] M. E. Madjet, H. S. Chakraborty, and S. T. Manson, *Phys. Rev. Lett.* **99**, 243003 (2007).
- [14] T. Greber, O. Raetz, T. J. Kreutz, P. Schwaller, W. Deichmann, E. Wetli, and J. Osterwalder, *Rev. Sci. Instrum.* **68**, 4549 (1997).
- [15] J. Osterwalder, T. Greber, A. Stuck, and L. Schlapbach, *Phys. Rev. B* **44**, 13764 (1991).
- [16] R. Ahlrichs, M. Bär, M. Häser, H. Horn, and C. Kölmel, *Chem. Phys. Lett.* **162**, 165 (1989).
- [17] A. Schäfer, C. Huber, and R. Ahlrichs, *J. Chem. Phys.* **100**, 5829 (1994).
- [18] PBE0 is a hybrid functional in which 25% of Hartree-Fock exchange is mixed into the generalised gradient approximation by Perdew, Burke and Ernzerhof [J. P. Perdew, K. Burke and M. Ernzerhof, *Phys. Rev. Lett.* **77**, 3865 (1996)].
- [19] B. A. DiCamillo, R. L. Hettich, G. Guiochon, R. N. Compton, M. Saunders, H. A. Jiménez-Vázquez, A. Khong, and R. J. Cross, *J. Phys. Chem.* **100**, 9197 (1996).
- [20] U. Hergenhahn, S. Barth, V. Ulrich, M. Mücke, S. Joshi, T. Lischke, A. Lindblad, T. Rander, G. Öhrwall, and O. Björneholm, *Phys. Rev. B* **79**, 155448 (2009).
- [21] K. Jacobi, *Phys. Rev. B* **38**, 5869 (1988).
- [22] P. J. Benning, D. M. Poirier, N. Troullier, J. L. Martins, J. H. Weaver, R. E. Haufler, L. P. F. Chibante, and R. E. Smalley, *Phys. Rev. B* **44**, 1962 (1991).
- [23] T. Liebsch, O. Plotzke, F. Heiser, U. Hergenhahn, O. Hemmers, R. Wehlitz, J. Viehhaus, B. Langer, S. B. Whitfield, and U. Becker, *Phys. Rev. A* **52**, 457 (1995).
- [24] A. Rüdél, R. Hentges, U. Becker, H. S. Chakraborty, M. E. Madjet, and J. M. Rost, *Phys. Rev. Lett.* **89**, 125503 (2002).
- [25] P. Colavita, G. De Alti, G. Fronzoni, M. Stener, and P. Decleva, *Phys. Chem. Chem. Phys.* **3**, 4481 (2001).
- [26] S. Korica, D. Rolles, A. Reinköster, B. Langer, J. Viehhaus, S. Cvejanović, and U. Becker, *Phys. Rev. A* **71**, 013203 (2005).
- [27] S. Korica, Ph.D. thesis, Technische Universität Berlin, 2006.
- [28] J. J. Yeh and I. Lindau, *At. Data Nucl. Data Tables* **32**, 1 (1985).
- [29] I. V. Hertel, H. Steger, J. de Vries, B. Weisser, C. Menzel, B. Kamke, and W. Kamke, *Phys. Rev. Lett.* **68**, 784 (1992).